

μ SR study of superconducting Re-B compounds

S. Sharma,¹ Arushi,² K. Motla,² J. Beare,¹ M. Nugent,¹ M. Pula,¹
T.J. Munsie,³ A. D. Hillier,⁴ R. P. Singh,² and G. M. Luke^{1,5,*}

¹*Department of Physics and Astronomy, McMaster University, Hamilton, Ontario L8S 4M1, Canada*

²*Department of Physics, Indian Institute of Science Education and Research Bhopal, Bhopal, 462066, India*

³*Defence Research and Development Canada, Suffield Research Centre, Ralston, Alberta T0J 2N0, Canada*

⁴*ISIS Facility, STFC Rutherford Appleton Laboratory,*

Harwell Science and Innovation Campus, Oxfordshire, OX11 0QX, UK

⁵*TRIUMF, Vancouver, British Columbia V6T 2A3, Canada*

(Dated: March 27, 2022)

We present a self-consistent determination of superconducting properties of Re_7B_3 and Re_3B through specific heat, magnetic susceptibility, resistivity, and transverse and zero-field muon spin rotation/relaxation (μ SR) experiments on polycrystalline samples. Re_7B_3 ($T_C = 3.2$ K) is a non-centrosymmetric type-II ($\kappa \simeq 9.27$) superconductor in the weak coupling ($\lambda_{e-ph} = 0.54$) regime. On the other hand, Re_3B ($T_C = 5.19$ K) is a centrosymmetric type-II ($\kappa \simeq 34.55$) superconductor in the moderate coupling ($\lambda_{e-ph} = 0.64$) regime. Our transverse-field μ SR measurements show evidence for isotropically gaped BCS type superconductivity with normalized gap ($\Delta_0/k_B T_C$) values of 1.69 (Re_7B_3) and 1.75 (Re_3B).

I. INTRODUCTION

Symmetry breaking in phase transitions is a central concept in physics and superconductivity is a good phenomenon which demonstrates it. Conventional superconductors break gauge symmetry while unconventional superfluids and superconductors can break other kinds of symmetries. It was after the discovery of unconventional superconductivity in inversion symmetry lacking CePt_3Si [1], that non-centrosymmetric superconductors (NCS) jumped into the limelight. The lack of inversion symmetry gives rise to an anti-symmetric spin-orbital coupling, which can lead to an admixture of the spin-singlet and spin-triplet Cooper pairs [2–4]. The mixed-pairing state can prompt non-centrosymmetric superconductors to manifest remarkably different properties from conventional BCS superconductors: for example, point or line nodes in the superconducting gap function [5–8], presence of multiple superconducting gaps [7, 9], Pauli limit exceeding upper critical fields [1, 10–13], topologically protected zero-energy surface bands [14], and time-reversal symmetry (TRS) breaking [15, 16]. The non-centrosymmetry and existence of TRS breaking in La_7Ir_3 [17] makes a good case for iso-structural Re_7B_3 to show TRS breaking and hence, unconventional superconductivity.

There have been many cases of Re based non-centrosymmetric superconductors exhibiting unconventional superconducting properties [16, 18, 19]. The recent discovery of TRS breaking fields in centrosymmetric elemental Re [20] has ignited fresh interest in Re based superconductors. Since the TRS breaking in ReT ($X =$

transition metal) alloys is attributed to Re, Re_3B (centrosymmetric space group Cmcm) due to its high Re content, also becomes an interesting candidate for exhibiting TRS breaking. This can also help identify the existence of a critical Re concentration beyond which a compound will show TRS breaking. Through the study of these compounds, we can better understand the relative importance of Re concentration and non-centrosymmetry in TRS breaking/unconventionality.

Although there have been some studies using micro and macroscopic techniques in their normal state [21] as well as superconducting state [22–24], there is not much information about the symmetry of the superconducting gap and possible presence of TRS breaking fields of Re_7B_3 and Re_3B . In this paper, we report the superconducting properties of these compounds, through magnetization, resistivity, specific heat, and muon spin rotation/relaxation (μ SR) measurements.

II. EXPERIMENTAL DETAILS

Our samples were synthesized by repeatedly arc melting Re (99.9%) and 5% excess B (99.9%) in a high purity argon atmosphere carefully flipping the ingot before each melting. A small portion of the sample was powdered and characterized with an X'pert PANalytical x-ray diffractometer ($\text{Cu-K}\alpha$ radiation, $\lambda = 1.540$ Å) to confirm the phase purity of the samples.

The superconducting properties of both Re_7B_3 and Re_3B were measured using specific heat, magnetization, resistivity, and muon spin relaxation/rotation (μ SR) measurements. Magnetization measurements were carried out in Quantum Design MPMS-3 SQUID magnetometer [25]. The specific heat and resistivity data were obtained using a Quantum Design Physical Property

* luke@mcmaster.ca

Measurement System (PPMS). μ SR measurements were performed at the M15 beamline of TRIUMF's Center for Molecular and Materials Science, Vancouver, which was equipped with a dilution refrigerator. In the transverse-field geometry, the spins of the implanted muons are initially perpendicular to the magnetic field applied to the sample. At the M15 beamline, the magnetic field was parallel to the beam axis, and therefore, to achieve TF geometry, the muon spins were rotated before implantation, leading to the use of left and right detectors for asymmetry measurement as a function of time. The polycrystalline samples were cut into plates with a diamond saw before mounting on the silver sample holder (cold finger). Copper grease was used to fix the plates on the sample holder which was wrapped by a thin silver foil to ensure good thermal contact.

We performed zero-field muon spin relaxation experiments to detect possible spontaneous fields in the superconducting state. This required zeroing of the stray field into the sample space, which involved very accurate measurement of the field and subsequent application of the negative field by perpendicular magnets. The zero-field environment (accurate to $2 \mu\text{T}$) was achieved by following the procedure described by Morris et. al. [26].

III. RESULTS AND DISCUSSION

Resistivity Fig. 1 (c-d) depicts the superconducting transitions on the resistivity data. $T_{C,mid}$ is the temperature at the midpoint of the resistivity drop. Re_7B_3 transitions to the superconducting state at $T_{C,mid} = 3.3 \text{ K}$ while Re_3B transitions at $T_{C,mid} = 4.8 \text{ K}$. We fitted the normal state resistivity data with $\rho = \rho_0 + \rho_1 T^2$ to compute the normal state residual resistivity, ρ_0 , obtaining $1.86 \pm 0.01 \mu\Omega\text{cm}$ and $65.38 \pm 0.09 \mu\Omega\text{cm}$ for Re_7B_3 and Re_3B , respectively, which in turn was used to estimate the mean free path of the electrons, l .

Magnetization Fig. 1 (a-b) depicts the magnetic susceptibility data with T_C onset of 3.2 K and 5.19 K for Re_7B_3 and Re_3B , respectively. The shielding volume fraction is close to 100 % indicating the full spread of superconductivity within the samples. The higher susceptibility in the ZFCW case implies the presence of flux pinning and the value lower than -1 likely reflects the lower sample density than the one used in the calculation.

The inset of the Fig. 2 shows the magnetization versus field curves at different temperatures. The magnetic flux starts penetrating the sample at lower critical field (H_{C1}) which leads to non linear behavior of magnetization for post H_{C1} fields. The H_{C1} was extracted from the magnetization isotherms and modeled using the Ginzburg-Landau Eq. 1 to determine the $H_{C1}(0)$, the lower critical field at 0 K. The $H_{C1}(0)$ for Re_7B_3 and Re_3B were obtained to be $9.98 \pm 0.08 \text{ mT}$ and $4.05 \pm 0.03 \text{ mT}$,

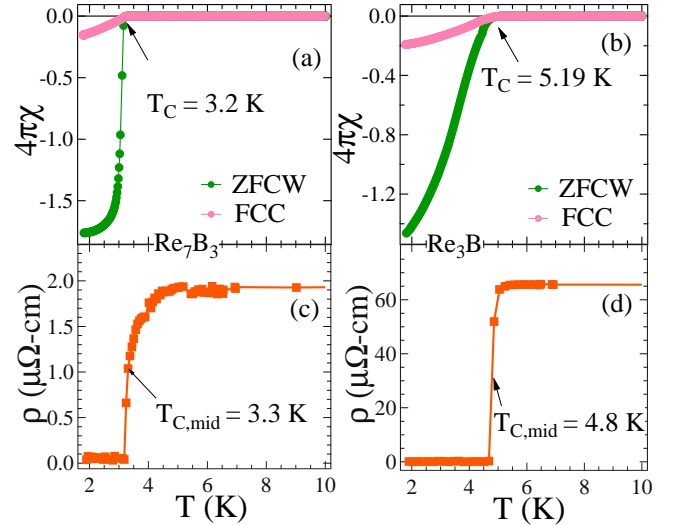


FIG. 1. The top half of the figure shows zero-field cooled warming (ZFCW) and field cooled cooling (FCC) volume magnetic susceptibility data in 10 G field for (a) Re_7B_3 and (b) Re_3B . The lower half of the figure shows zero-field resistivity data with superconducting transitions at 3.3 K and 4.8 K for (c) Re_7B_3 and (d) Re_3B , respectively, slightly different from the values obtained through the magnetic susceptibility data.

respectively.

$$H_{C1}(T) = H_{C1}(0) \left[1 - \left(\frac{T}{T_C} \right)^2 \right] \quad (1)$$

The magnetic susceptibility as a function of temperature for various applied fields for Re_3B is shown in the inset of Fig. 2 (a). Fig. 2 (b) shows the upper critical field values varying with reduced temperature which was extracted from the susceptibility curves for the respective samples. We used the Ginzburg-Landau model (Eq. 2), which is effective for temperatures close to T_C , to estimate the $H_{C2}(0)$ as shown in Fig. 2 (b).

$$H_{C2}(T) = H_{C2}(0) \left[\frac{1 - t^2}{1 + t^2} \right], \quad (2)$$

where $t = T/T_C$. H_{C2} is related to the Ginzburg-Landau coherence length (ξ_{GL}) through [27],

$$H_{C2}(0) = \frac{\phi_0}{2\pi\xi_{GL}^2}, \quad (3)$$

where $\phi_0 (=2.07 \times 10^{-15} \text{ Tm}^2)$ is the magnetic flux quantum. We calculated $\xi_{GL}(0)$ using our $H_{C2}(0)$ values, obtaining $20.68 \pm 0.12 \text{ nm}$ for Re_7B_3 and $11.13 \pm 0.08 \text{ nm}$ for Re_3B . The Ginzburg-Landau penetration depth (λ_{GL}) can also be calculated using the expression [27],

$$H_{C1}(0) = \frac{\phi_0}{4\pi\lambda_{GL}^2(0)} \left(\ln \frac{\lambda_{GL}(0)}{\xi_{GL}(0)} \right). \quad (4)$$

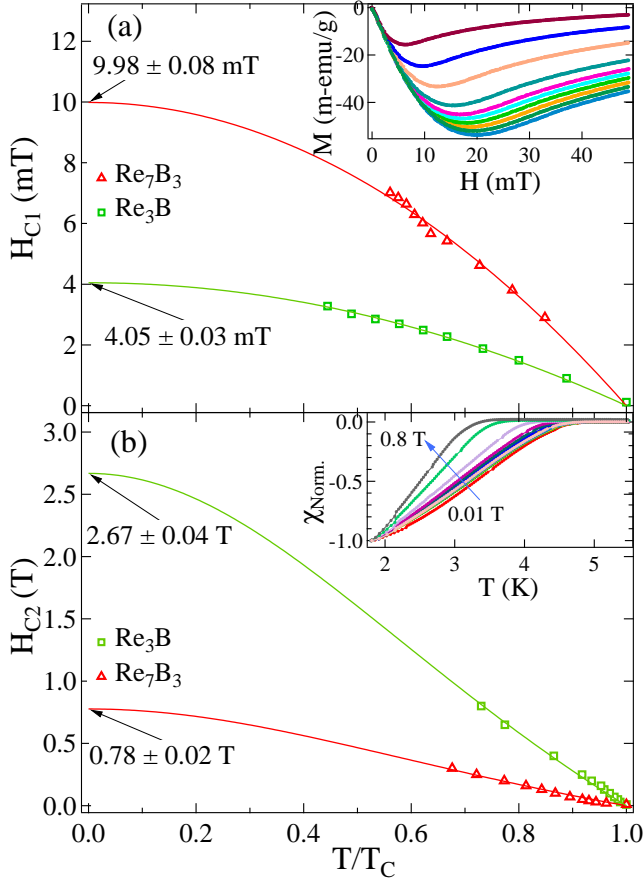


FIG. 2. (a). The lower critical field H_{C1} values were determined from the magnetization (M) versus field (H) curves at various temperatures [Inset]. The red and green lines represent the $H_{C1}(T)$ data as modeled using the Ginzburg-Landau theory (Eq. 2). $H_{C1}(0)$ values obtained from the fits are shown in the figure [Tagged arrow]. (b). Magnetic susceptibility (χ) versus temperature (T) is plotted at various fields for Re_3B [Inset]. The upper critical field (H_{C2}) values as a function of temperature (T) as determined from χ versus T graph are plotted. The red and green line represent the fits of the data in accordance with the Ginzburg-Landau theory (Eq. 1).

Using values of $H_{C1}(0)$ from Fig. 2 (a) and $\xi_{GL}(0)$, we obtained $\lambda_{GL}(0)$ values for Re_7B_3 and Re_3B , which are 191.88 ± 1.34 nm and 384.51 ± 1.53 nm, respectively. We can determine the thermodynamic critical field $H_C(0)$ using the $\xi_{GL}(0)$ and $\lambda_{GL}(0)$ values using the equation,

$$H_C(0) = \frac{\phi_0}{2\sqrt{2}\lambda_{GL}(0)\xi_{GL}(0)}. \quad (5)$$

The $H_C(0)$ for Re_7B_3 is 0.184 ± 0.002 T while for Re_3B it is 0.171 ± 0.002 T.

The Ginzburg-Landau parameter $\kappa = \lambda_{GL}/\xi_{GL}$ can be calculated, giving 9.28 ± 0.12 for Re_7B_3 and 34.55 ± 0.38 for Re_3B . The $\kappa > 1/\sqrt{2}$ as expected as both these compounds are type-II superconductors.

Specific heat Specific heat data for Re_7B_3 and Re_3B are shown in Fig. 3. The dotted green line represents the

fit to the specific heat data above T_C . The lattice contribution to the heat capacity above T_C can be written as $\beta_3 T^3 + \beta_5 T^5$ while the electronic portion is given by $\gamma_n T$. The specific heat (C) divided by temperature (T) was fitted with $C/T = \gamma_n + \beta_3 T^2 + \beta_5 T^4$ as shown in insets of Fig. 3 (a, b). Here, γ_n is the Sommerfeld coefficient and, β_3 and β_5 are the coefficients of the phononic contribution. From the fits of Re_7B_3 , we obtained $\gamma_n = 20.61 \pm 0.80$ mJ/mol-K², $\beta_3 = 0.42 \pm 0.03$ mJ/mol-K⁴ and $\beta_5 = 2.66 \pm 0.19$ μ J/mol-K⁶. Whereas, for Re_3B we obtained, $\gamma_n = 9.86 \pm 0.27$ mJ/mol-K², $\beta_3 = 0.38 \pm 0.01$ mJ/mol-K⁴ and $\beta_5 = 0$ (imposed).

We can estimate the Debye temperatures (θ_D) with the help of β_3 using [28],

$$\theta_D = \left(\frac{12\pi^4 R N}{5\beta_3} \right)^{\frac{1}{3}}, \quad (6)$$

where R is the gas constant and N is the number of atoms per formula unit. We obtained $\theta_D = 359$ K, 274 K for Re_7B_3 and Re_3B , respectively. Similarly, for non interacting particles, the γ_n relates to the density of states at Fermi level $D_C(E_f)$ through $\gamma_n = (\pi^2 k_B^2 / 3) \times D_C(E_f)$. This yields $D_C(E_f) = 8.73 \pm 0.34$ $\frac{\text{States}}{\text{eV f.u.}}$ for Re_7B_3 and $D_C(E_f) = 4.17 \pm 0.11$ $\frac{\text{States}}{\text{eV f.u.}}$ for Re_3B .

We can determine the electron-phonon coupling constant (λ_{e-ph}) using the McMillan theory [29]. λ_{e-ph} gives the strength of the attractive interaction between the

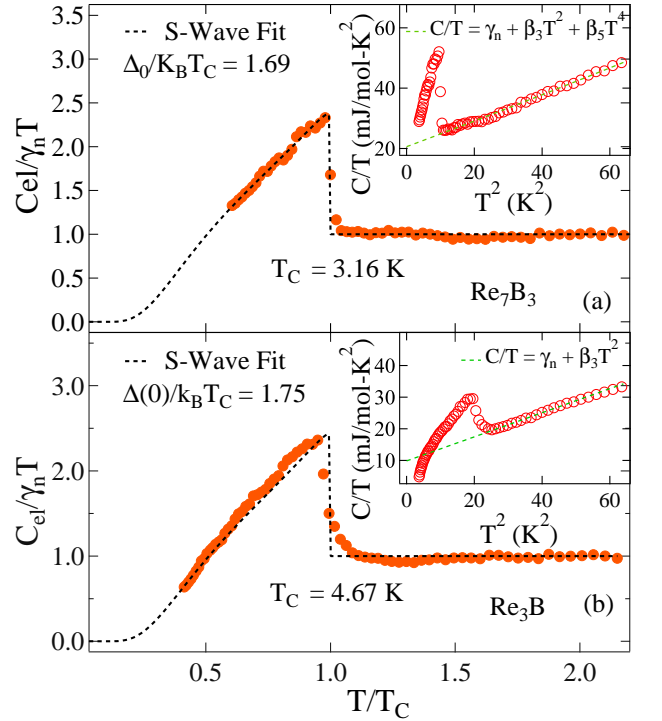


FIG. 3. The normalized electronic specific heat and its fit to the isotropic BCS model for (a) Re_7B_3 and (b) Re_3B . Insets: C/T plotted against T^2 where the dotted green line represents the fits to the normal state specific heat.

electrons due to the interaction with the lattice. The following expression involves θ_D , T_C and the residual screened Coulomb interaction parameter (μ^*).

$$\lambda_{e-ph} = \frac{1.04 + \mu^* \ln(\theta_D/1.45T_C)}{(1 - 0.062\mu^*) \ln(1 - 0.062\mu^*) - 1.04} \quad (7)$$

where μ^* can be assumed to be 0.13 as for many inter-metallic superconductors [29]. The λ_{e-ph} values obtained for Re_7B_3 (0.54) is close to other weak coupling non-centrosymmetric superconductors like TaOs [30]. For Re_3B , the value of λ_{e-ph} (0.64) is comparable to other moderately coupled superconductors like Re_6Hf (0.63) [31], $\text{Re}_{24}\text{Ti}_5$ (0.6) [32, 33], and Re_3Ta (0.62) [34] suggesting moderately strong coupling in Re_3B .

The electronic portion of the heat capacity (C_{el}) can be obtained by subtracting the phononic contribution (C_{ph}) from the total heat capacity. The electronic heat capacity can be computed from the entropy using the thermodynamic relation [27],

$$\frac{S}{\gamma_n T_C} = \frac{-6}{\pi^2 k_B T_C} \int_0^\infty [(1-f) \ln(1-f) + f \ln f] d\xi, \quad (8)$$

where $f = (1 + e^{E/K_B T})^{-1}$ and ξ is the energy of the normal electrons relative to the Fermi energy. The fermion excitation energy can be written as $E(\xi) = [\xi^2 + \Delta^2(t)]^{1/2}$ where energy gap, Δ , has temperature dependence in accordance with the BCS approximation [35],

$$\Delta(t) = \Delta_0 \tanh(1.82\{1.018[(T_C/T) - 1]\}^{0.51}), \quad (9)$$

where Δ_0 is the Δ at zero temperature. The normalized electronic heat capacity ($C_{el}/\gamma_n T$) is plotted against the reduced temperature (T/T_C) in Fig. 3 (a) and (c). The dotted black line is the fit of the α model [36], derived from BCS theory, for an isotropic gap superconductor as described above. The values of $\alpha = \Delta_0/k_B T_C$, the normalized gap, as obtained from the fits are 1.69 for Re_7B_3 and 1.75 for Re_3B . These values are slightly smaller but very close to the BCS value $\alpha_{BCS} = \Delta_0/k_B T_C = 1.764$. The specific heat jump ($C_{el}/\gamma_n T_C$) at T_C , as determined from the specific heat plots are $\simeq 1.348$ for Re_7B_3 and $\simeq 1.428$ for Re_3B . Both these values are also strikingly close to the BCS value (1.43) for conventional s-wave superconductors.

Zero-field (ZF) muon spin relaxation/rotation (μSR)
We performed the ZF- μSR measurements to search for possible small spontaneous fields associated with the time-reversal symmetry breaking (TRSB) in the superconducting state. To investigate the change in internal fields between normal and superconducting state, we recorded the asymmetry spectra at several temperature points on both sides of the transition temperature and modeled it with the static Gaussian Kubo-Toyabe (KT) Eq. 10. The Gaussian KT model [37] describes the relaxation due to a Gaussian distribution of random fields

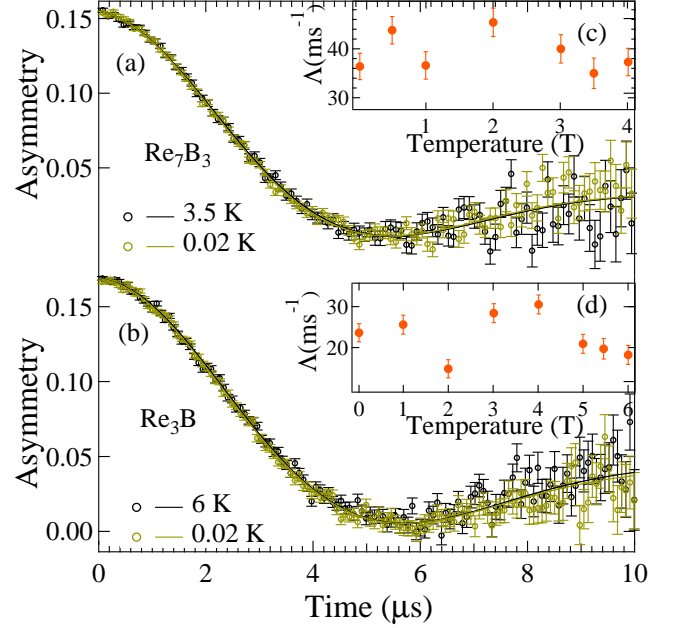


FIG. 4. (a) The representative zero-field spectra from Re_7B_3 in normal state ($T = 3.5\text{ K}$) and superconducting state ($T = 20\text{ mK}$). (b) The ZF spectra obtained from Re_3B in normal state ($T = 6\text{ K}$) and superconducting state ($T = 20\text{ mK}$). (c) and (d) represent the electronic relaxation rate (Λ) obtained from the fits.

appropriate for densely packed random moments arising from nuclear dipoles.

$$G_{KT}(t) = \frac{1}{3} + \frac{2}{3}(1 - \sigma_{ZF}^2) \exp\left(\frac{-\sigma_{ZF}^2 t^2}{2}\right) \quad (10)$$

where σ_{ZF} is relaxation due to the static and randomly oriented nuclear dipole moments located in the vicinity of the muon site. σ_{ZF}/γ_μ is the width of the local field distribution and γ_μ is the gyromagnetic ratio. The complete asymmetry spectra was fitted using the expression

$$A(t) = A_1 G_{KT} \exp(-\Lambda t) + A_{BG}, \quad (11)$$

where A_1 is the asymmetry of the sample signal. A_{BG} is the asymmetry contributed by the background. The exponential relaxation ($e^{-\Lambda t}$) accounts for the relaxation due to possible spontaneous fields. This model was used to fit the asymmetry spectra collected at various temperatures on either side of T_C and the resultant values of electronic relaxation rate (Λ) are depicted in the insets of Fig. 4. The fits of the asymmetry spectra trace almost the same function as we can see in Fig. 4 (a-b). The Gaussian relaxation rate (σ_{ZF}) largely remained constant for different temperature scans and therefore, it was made a global variable during the fits. The values of σ_{ZF} obtained for Re_7B_3 and Re_3B are $0.320 \pm 0.001\text{ }\mu\text{s}^{-1}$ and $0.304 \pm 0.001\text{ }\mu\text{s}^{-1}$, respectively, which corresponds to nuclear dipole fields of $\simeq 3.76\text{ G}$ and $\simeq 3.57\text{ G}$. In addition, there is no visible trend in the Λ down to the lowest

temperature, rather, the Λ values merely scatter around a temperature independent average value. The rms deviations of the Λ corresponds to the fields of 0.083 G and 0.075 G for Re_7B_3 and Re_3B , respectively, which corresponds to an upper limit of any spontaneous magnetic field roughly $1/50^{\text{th}}$ of the size of the nuclear dipole fields. These limits are smaller than most of the typical fields seen in TRS breaking superconductors between 0.1 and 0.5 G [38, 39]. However, we do note that we cannot exclude TRS breaking fields less than about 0.1 G as has been seen in few superconductors [19, 40].

Our results support the inferences made by Shang et. al. [41] on the importance of critical rhenium concentration for TRS breaking in Re based alloys. Both Re_3B and Re_7B_3 , due to their relatively low rhenium content, do not show any evidence of TRS breaking irrespective of the presence or absence of inversion symmetry in their crystal structure. This is in line with the recent work on iso-stoichiometric Re_3W [42] which exists in both centrosymmetric and non-centrosymmetric crystal structures and preserves time-reversal symmetry.

Transverse-field (TF) muon spin relaxation/rotation (μSR) For TF μSR experiment, samples were cooled in the fields 100 mT and 760 mT for Re_7B_3 and Re_3B , respectively, which is well above their lower critical fields (H_{C1}). Asymmetry spectra were recorded above and below the superconducting transition temperatures. Rotating reference frame (rrf) plots of the asymmetry spectra are shown in Fig. 5 (a-b). The rrf field for Re_7B_3 and Re_3B was 90 mT and 750 mT, respectively.

The TF- μSR asymmetry signal decays with time due to the in-homogeneous field distribution due to the underlying flux line lattice (FLL) below T_C . Above T_C the depolarization rate is lower but nonzero due to the Gaussian field distribution of randomly oriented nuclear dipole moments. The time evolution of asymmetry can be described using two sinusoidally oscillating terms with Gaussian and exponential relaxation terms multiplied to it for sample and background (Ag Sample holder) part of the signal, respectively.

$$G_{TF}(t) = A[(1 - F)e^{-\psi t} \cos(\omega_{bg}t + \phi) + (F)e^{\left(\frac{-\sigma^2 t^2}{2}\right)} \cos(\omega t + \phi)], \quad (12)$$

where ω and ω_{bg} are the frequencies of the muon precision signal in the sample and background, respectively. F is the fraction of the signal coming from the sample. A is the asymmetry and ϕ is the initial phase of muons entering the sample. σ and ψ are the sample and background depolarization rates, respectively. The ψ value obtained from TF fits for Re_7B_3 is zero whereas for Re_3B it is $0.15 \mu\text{S}^{-1}$. The temperature dependence of the depolarization/relaxation rate is obtained from the fits of the asymmetry spectra recorded at various temperatures as shown in Fig. 5(c-d).

In the case of superconductors, the muon depolarization rate (σ) consists of temperature independent back-

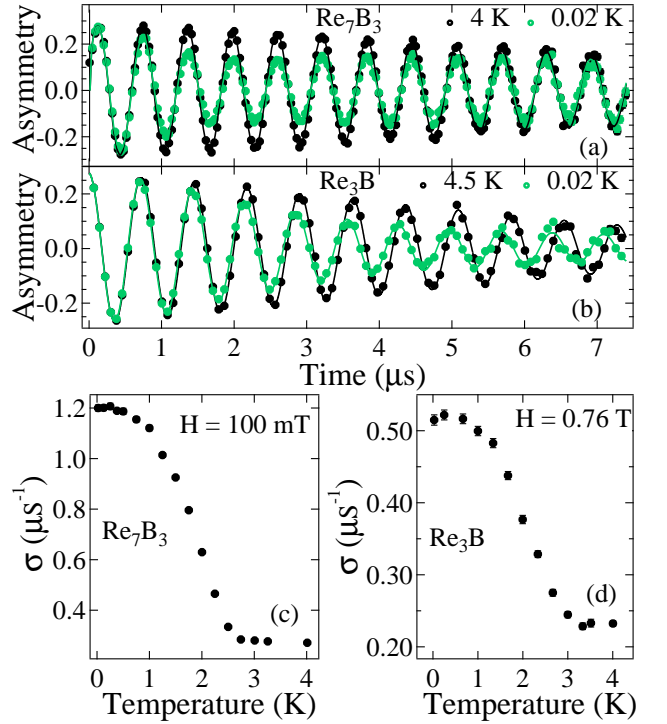


FIG. 5. (a) The representative transverse-field (TF) μSR asymmetry spectra modified in a rotating reference frame with frequency (a) $\gamma_\mu 90$ mT for Re_7B_3 (b) $\gamma_\mu 750$ mT for Re_3B depicts the difference in relaxation rates (σ) between normal and superconducting state. The sample relaxation rate (σ) and internal field at the muon site (H_{int}) as obtained from the asymmetry data fits are plotted in (c) & (d) for Re_7B_3 and (d) & (f) for Re_3B .

ground rate (σ_{bg}) and temperature dependent superconducting rate (σ_{sc}), $\sigma = \sqrt{\sigma_{bg}^2 + \sigma_{sc}^2}$. The superconducting depolarization rate (σ_{sc}) is the measure of the mean square in-homogeneity in the field, $\langle(\Delta B^2)\rangle$, sampled by the muons due to the underlying flux line lattice [43], where, $\langle(\Delta B)^2\rangle = \langle(B - \langle B \rangle)^2\rangle$. The depolarization rate for vortex lattice is given by

$$\sigma_{sc} = \langle(\Delta B)^2\rangle / \gamma_\mu, \quad (13)$$

where γ_μ ($= 2\pi \times 135.5$ MHz/T) is gyromagnetic ratio of the muon. We can use $\sigma_{sc}(T)$ to calculate the penetration depth (λ) as a function temperature. Brandt's approximation for the Abrikosov solution of the linearized GL theory gives Eq. 14, which works well for the field range examined for Re_3B .

$$\frac{1}{\lambda^2(T)} = \frac{5.814 \times \sigma_{sc}(T)}{\gamma_\mu \Phi_0 (1 - h) [1 + 1.21(1 - \sqrt{h})^3]} \quad (14)$$

where Φ_0 is the magnetic flux quantum and h , H/H_{C2} , is temperature dependent reduced field. For Re_7B_3 the ratio H/H_{C2} is very small and therefore, λ can be ex-

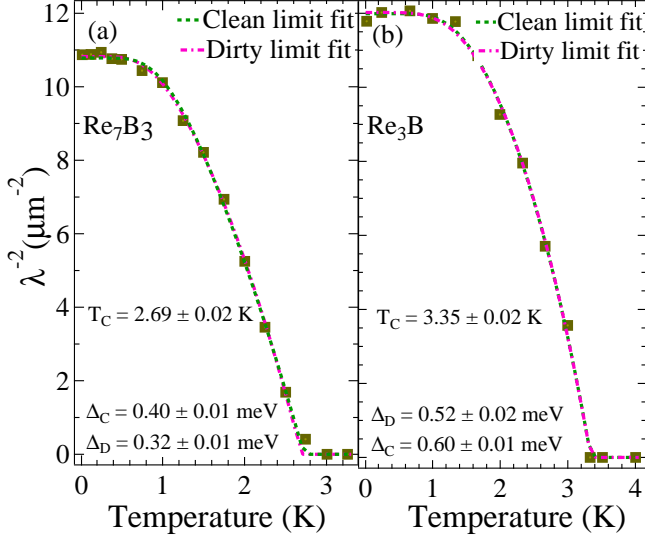


FIG. 6. The graphs depicts the temperature dependence of inverse square penetration depth data calculated using (a) Eq. 15 for Re_7B_3 (b) Eq. 14 for Re_3B . The green and pink dotted lines represent the clean and dirty limit BCS fits of the data.

tracted using the simplified expression [44],

$$\frac{1}{\lambda^2(T)} = \frac{\sigma_{sc}(T)}{0.061 \times \gamma_\mu \Phi_0}. \quad (15)$$

We can get more insight into the nature of the superconducting gap by modeling the London penetration depth obtained earlier, with the s-wave BCS superconductor model. This requires the knowledge of whether the superconductor is in the clean or dirty limit, which can be done by estimating the ratio of coherence length to the quasiparticle mean free path, ξ/l . If ξ/l is a number much less than one, then the superconductor is considered to be in the clean limit. We estimated this ratio using the eq. 17-19 from Arushi et. al. [13]. We find that both Re_7B_3 and Re_3B are clean limit superconductors with $\xi/l = 0.09$ and 0.40 , respectively.

In the clean limit, the London penetration depth (λ) can be fitted using the equation,

$$\frac{\lambda^{-2}(T)}{\lambda^{-2}(0)} = 1 + 2 \int_{\Delta(T)}^{\infty} \frac{\partial f}{\partial E} \frac{EdE}{\sqrt{E^2 - \Delta(T)}}, \quad (16)$$

where $f = [1 + \exp(E/k_B T)]^{-1}$ and $\Delta(T)$ is given by Eq. 9. For completeness, we can fit the results in the dirty limit as well, noting that we used normal state estimate for mean free path. In the dirty local limit within the London approximation, we can write

$$\frac{\lambda^{-2}(T)}{\lambda^{-2}(0)} = \frac{\Delta(T)}{\Delta(0)} \tanh \left[\frac{\Delta(T)}{2k_B T} \right], \quad (17)$$

where $\Delta(T)$ is given by Eq. 9, the BCS approximation for the energy gap. The fits of the data in the two regimes

TABLE I. Table presenting the superconducting and normal state parameter values for Re_7B_3 and Re_3B .

Parameter	unit	Re_7B_3	Re_3B
T_C	K	3.2	5.19
$H_{C1}(0)$	Oe	99.8	39.47
$H_{C2}(0)$	T	0.77	2.66
$H_C(0)$	T	0.184	0.171
$\xi_{GL}(0)$	nm	20.68	11.13
Λ_{e-ph}		0.54	0.64
$\Lambda_{GL}(0)$	nm	198.18	384.51
k_{GL}		9.277	34.55
γ_n	$mJ/mole - K^2$	20.607	9.856
θ_D	K	359	274
ξ/l		0.09	0.40
$\Delta C_{el}/\gamma_n T_C$		1.348	1.428
$\Delta_0/k_B T_C^a$		1.69	1.75
$\Delta_0/k_B T_C^b$		1.72	2.07
$\Delta_0/k_B T_C^c$		1.36	1.80

^a Specific heat

^b TF μSR (clean limit)

^c TF μSR (dirty limit)

are plotted in Fig. 6. Both, clean and dirty limit fits are indistinguishable and fit the data well, implying the absence of nodes in superconducting gap for both.

For Re_7B_3 , the dirty limit BCS fit yields $\Delta_D(0) = 0.32 \pm 0.01$ meV while the clean limit fit yields $\Delta_C(0) = 0.40 \pm 0.01$ meV. Consequently, the normalized gap values are $\Delta_D/k_B T_C$ (1.36 ± 0.04) and $\Delta_C/k_B T_C$ (1.72 ± 0.05). Similarly, the dirty limit fit for Re_3B gives $\Delta_D(0) = 0.52 \pm 0.02$ meV while the clean limit fit yields $\Delta_C(0) = 0.60 \pm 0.01$ meV. The reduced gap values comes out to be $\Delta_D/k_B T_C$ (1.80 ± 0.08) and $\Delta_C/k_B T_C$ (2.07 ± 0.05).

IV. CONCLUSION

We carried out detailed resistivity, magnetization, specific heat, TF- μSR , and ZF- μSr measurements on polycrystalline samples of Re_7B_3 and Re_3B . The comparison of their various superconducting and normal state parameters derived from the above measurements are listed down in Table I. Re_7B_3 is a weakly coupled superconductor while Re_3B is a moderately coupled superconductor. Both Re_7B_3 and Re_3B show conventional s-wave superconductivity with superconducting gaps of 0.40 ± 0.02 meV and 0.60 ± 0.02 meV, respectively in the clean limit. We find no evidence for TRS breaking; the magnitude of the maximum possible TRS breaking fields that might go undetected in Re_7B_3 ($7.5 \mu\text{T}$) and Re_3B ($8.3 \mu\text{T}$) are small in comparison to many TRS breaking superconductors ($10 \mu\text{T} - 50 \mu\text{T}$) [38, 39]. Therefore, despite having many ingredients for unconventional superconductivity, Re_3B and Re_7B_3 seem to be quite con-

ventional.

V. ACKNOWLEDGEMENTS

We would like to thank B.S. Hitti, S. Dunsiger, and G.D. Morris for their assistance during the μ SR measurements. Work at McMaster was supported by the Natural Sciences and Engineering Research Council of Canada. R. P. S. acknowledges the Science and Engineering Research Board, Government of India for the Core Research Grant CRG/2019/001028. Financial support from DSTFIST Project No. SR/FST/PSI-195/2014(C) is also thankfully acknowledged.

-
- [1] E. Bauer, G. Hilscher, H. Michor, C. Paul, E. W. Scheidt, A. Griбанov, Y. Seropegin, H. Noël, M. Sigrist, and P. Rogl, Heavy Fermion Superconductivity and Magnetic Order in Noncentrosymmetric CePt₃Si, *Physical Review Letters* **92**, [10.1103/PhysRevLett.92.027003](#) (2004).
 - [2] M. Smidman, M. B. Salamon, H. Q. Yuan, and D. F. Agterberg, Superconductivity and spin-orbit coupling in non-centrosymmetric materials: a review, *Reports on Progress in Physics* [10.1088/1361-6633/80/3/036501](#) (2017).
 - [3] L. P. Gor'kov and E. I. Rashba, Superconducting 2D System with Lifted Spin Degeneracy: Mixed Singlet-Triplet State, *Physical Review Letters* **87**, [10.1103/PhysRevLett.87.037004](#) (2001).
 - [4] H. Q. Yuan, D. F. Agterberg, N. Hayashi, P. Badica, D. Vandervelde, K. Togano, M. Sigrist, and M. B. Salamon, S-Wave Spin-Triplet Order in Superconductors without Inversion Symmetry: Li₂Pd₃B and Li₂Pt₃B, *Physical Review Letters* **97**, [10.1103/PhysRevLett.97.017006](#) (2006).
 - [5] H. Takeya, M. ElMassalami, S. Kasahara, and K. Hirata, Specific-heat studies of the spin-orbit interaction in noncentrosymmetric Li₂(Pd_{1-x}Pt_x)₃B ($x = 0, 0.5, 1$) superconductors, *Physical Review Letters* **76**, [10.1103/PhysRevB.76.104506](#) (2007).
 - [6] J. Chen, M. B. Salamon, S. Akutagawa, J. Akimitsu, J. Singleton, J. L. Zhang, L. Jiao, and H. Q. Yuan, Evidence of nodal gap structure in the noncentrosymmetric superconductor Y₂C₃, *Physical Review B* **83**, 144529 (2011).
 - [7] S. Kuroiwa, Y. Saura, J. Akimitsu, M. Hiraishi, M. Miyazaki, K. H. Satoh, S. Takeshita, and R. Kadono, Multigap Superconductivity in Sesquicarbides La₂C₃ and Y₂C₃, *Physical Review Letters* **100**, [10.1103/PhysRevLett.100.097002](#) (2007).
 - [8] Y. T. Shao, X. X. Wu, L. Wang, Y. G. Shi, J. P. Hu, and J. L. Luo, Evidence of line nodes in superconducting gap function in K₂Cr₃As₃ from specific-heat measurements, *EPL* **123**, 57001 (2018).
 - [9] T. Shang, A. Amon, D. Kasinathan, W. Xie, M. Bobnar, Y. Chen, A. Wang, M. Shi, M. Medarde, H. Q. Yuan, and T. Shiroka, Enhanced T_c and multiband superconductivity in the fully-gapped ReBe₂₂ superconductor, *Physical Review B* [10.1088/1367-2630/ab307b](#) (2019).
 - [10] A. B. Karki, Y. M. Xiong, I. Vekhter, D. Browne, P. W. Adams, D. P. Young, K. R. Thomas, J. Y. Chan, H. Kim, and R. Prozorov, Structure and physical properties of the noncentrosymmetric superconductor Mo₃Al₂C, *Physical Review B* **82**, [10.1103/PhysRevB.82.064512](#) (2010).
 - [11] J.-K. Bao, J.-Y. Liu, C.-W. Ma, Z.-H. Meng, Z.-T. Tang, Y.-L. Sun, H.-F. Zhai, H. Jiang, H. Bai, C.-M. Feng, Z.-A. Xu, and G.-H. Cao, Superconductivity in Quasi-One-Dimensional K₂Cr₃As₃ with Significant Electron Correlations, *Physical Review X* [10.1103/PhysRevX.5.011013](#) (2015).
 - [12] N. Kimura, K. Ito, K. Saitoh, Y. Umeda, H. Aoki, and T. Terashima, Pressure-Induced Superconductivity in Noncentrosymmetric Heavy-Fermion CeRhSi₃, *Physical Review Letters* **95**, [10.1103/PhysRevLett.95.247004](#) (2005).
 - [13] Arushi, D. Singh, P. K. Biswas, A. D. Hillier, and R. P. Singh, Unconventional superconducting properties of noncentrosymmetric Re_{5.5}Ta, *Physical Review B* **101**, 144508 (2020).
 - [14] P. M. Brydon, A. P. Schnyder, and C. Timm, Topologically protected flat zero-energy surface bands in noncentrosymmetric superconductors, *Physical Review B* **84**, 020501 (2011), [arXiv:1104.2257](#).
 - [15] A. D. Hillier, J. Quintanilla, and R. Cywinski, Evidence for Time-Reversal Symmetry Breaking in the Noncentrosymmetric Superconductor LaNiC₂, *Physical Review Letters* [10.1103/PhysRevLett.102.117007](#) (2009).
 - [16] D. Singh, S. K. P. J. A. T. Barker, D. McK Paul, A. D. Hillier, and R. P. Singh, Time-reversal symmetry breaking in the noncentrosymmetric superconductor Re₆Ti, *Physical Review B* **97**, 100505 (2018).
 - [17] J. A. T. Barker, D. Singh, A. Thamizhavel, A. D. Hillier, M. R. Lees, G. Balakrishnan, D. McK Paul, and R. P. Singh, Unconventional Superconductivity in La₇Ir₃ Revealed by Muon Spin Relaxation: Introducing a New Family of Noncentrosymmetric Superconductor That Breaks Time-Reversal Symmetry, *Physical Review Letters* [10.1103/PhysRevLett.115.267001](#) (2015).
 - [18] R. P. Singh, A. D. Hillier, B. Mazidian, J. Quintanilla, J. F. Annett, D. McK Paul, G. Balakrishnan, and M. R. Lees, Detection of Time-Reversal Symmetry Breaking in the Noncentrosymmetric Superconductor Re₆Zr Using Muon-Spin Spectroscopy, *Physical Review Letters* **112**, [10.1103/PhysRevLett.112.107002](#) (2013).
 - [19] D. Singh, J. A. T. Barker, A. Thamizhavel, D. McK Paul, A. D. Hillier, and R. P. Singh, Time-reversal symmetry breaking in the noncentrosymmetric superconductor Re₆Hf: Further evidence for unconventional behavior in the α -Mn family of materials, *Physical Review B-Rapid Communications* **96**, 180501 (2017).
 - [20] T. Shang, M. Smidman, S. K. Ghosh, C. Baines, L. J. Chang, D. J. Gawryluk, J. A. T. Barker, R. P. Singh, D. McK Paul, G. Balakrishnan, E. Pomjakushina, M. Shi, M. Medarde, A. D. Hillier, H. Q. Yuan, J. Quintanilla, J. Mesot, and T. Shiroka, Time-Reversal Symmetry Breaking in Re-Based Superconductors, *Physical Review Letters* **121**, 257002 (2018).
 - [21] C. S. Lue, Y. F. Tao, and T. H. Su, Comparative NMR investigation of the Re-based borides, *Physical Review B* **78**, 9 (2008).
 - [22] H. Takagiwa, A. Kawano, Y. Mizuta, T. Yamamoto, M. Yamada, K. Ohishi, T. Muranaka, J. Akimitsu, W. Higemoto, and R. Kadono, Magnetic penetration depth of a new boride superconductor Re₃B, *Physica B*

- Condensed Matter **326**, 355 (2003).
- [23] A. Kawano, Y. Mizuta, H. Takagiwa, T. Muranaka, and J. Akimitsu, The superconductivity in Re-B system, *Journal of the Physical Society of Japan* **72**, 1724 (2003).
 - [24] G. K. Strukova, V. F. Degtyareva, D. V. Shovkun, V. N. Zverev, V. M. Kiiko, A. M. Ionov, and A. N. Chaika, Superconductivity in the Re-B system, *arXiv* , 142432 (2001), [arXiv:0105293 \[cond-mat\]](#).
 - [25] Quantum Design USA, *Magnetic Property Measurement System ® MPMS 3 User's Manual Part Number 1500-100, F1*, Tech. Rep. (2016).
 - [26] G. D. Morris and R. H. Heffner, A method of achieving accurate zero-field conditions using muonium, *Physica B: Condensed Matter* **326**, 252 (2003).
 - [27] M. Tinkham, *Introduction to superconductivity (International series in pure and applied physics)*, 2nd ed., edited by E. Shira, Jack; Castellano (McGraw-Hill, Inc., 1996).
 - [28] C. P. Poole Jr., H. A. Farach, R. J. Creswick, and R. Prozorov, *Superconductivity*, 2nd ed. (Elsevier, 2007).
 - [29] W. L. Mcmillan, *Physical Review Letters*, Tech. Rep. 2 (Bell Telephone Laboratories, Murray Hill, New Jersey, New Jersey, 1967).
 - [30] D. Singh, K. P. Sajilesh, S. Marik, A. D. Hillier, and R. P. Singh, Superconducting properties of the noncentrosymmetric superconductor TaOs, *Superconducting Science and Technology* [10.1088/1361-6668/aa8f8e](#) (2017).
 - [31] D. Singh, A. D. Hillier, A. Thamizhavel, and R. P. Singh, Superconducting properties of the noncentrosymmetric superconductor Re₆Hf, *Physical Review B* **94**, 54515 (2016).
 - [32] T. Shang, G. M. Pang, C. Baines, W. B. Jiang, W. Xie, A. Wang, M. Medarde, E. Pomjakushina, M. Shi, J. Mesot, H. Q. Yuan, and T. Shiroka, Nodeless superconductivity and time-reversal symmetry breaking in the noncentrosymmetric superconductor Re₂₄ Ti₅, *Physical Review B* **97**, [10.1103/PhysRevB.97.020502](#) (2018).
 - [33] C. S. Lue, H. F. Liu, C. N. Kuo, P. S. Shih, J.-Y. Lin, Y. K. Kuo, M. W. Chu, T.-L. Hung, and Y. Y. Chen, Investigation of normal and superconducting states in noncentrosymmetric Re₂₄ Ti₅, *Supercond. Sci. Technol* **26**, 55011 (2013).
 - [34] J. A. T Barker, B. D. Breen, R. Hanson, A. D. Hillier, M. R. Lees, G. Balakrishnan, D. McK Paul, and R. P. Singh, Superconducting and normal-state properties of the noncentrosymmetric superconductor Re₃Ta, *Physical Review B* **98**, 104506 (2018).
 - [35] A. Carrington and F. Manzano, Magnetic penetration depth of MgB₂, *Physica C: Superconductivity and its Applications* **385**, 205 (2003).
 - [36] D. C. Johnston, Elaboration of the α -model derived from the BCS theory of superconductivity Related content Elaboration of the α -model derived from the BCS theory of superconductivity, *Superconductor Science and Technology* **26**, 18 (2013).
 - [37] R. S. Hayano, Y. J. Uemura, J. Imazato, N. Nishida, T. Yamazaki, and R. Kubo, *Physical Review B*, Tech. Rep. (1979).
 - [38] G. M. Luke, A. Keren, L. P. Le, W. D. Wu, Y. J. Uemura, D. A. Bonn, L. Taillefer, and D. Garrett, Muon Spin Relaxation in UPt₃, *Physical Review Letters* **71** (1993).
 - [39] G. Luke, Y. Fudamoto, K. Kojima, M. Larkin, J. Merrin, B. Nachumi, Y. Uemura, Y. Maeno, Z. Mao, Y. Mosri, H. Nakamura, and M. Sigrist, Time-reversal symmetry-breakingsuperconductivity in Sr₂RuO₄, *Nature* **258**, 748 (1998).
 - [40] J.-W. Zang, J. Zhang, Z.-H. Zhu, Z.-F. Ding, K. Huang, X.-R. Peng, A. D. Hillier, and L. Shu, Broken Time-Reversal Symmetry in Superconducting Partially Filled Skutterudite Pr₁ δ Pt₄ Ge₁₂ *, *Chinese Physics Letters* **36**, [10.1088/0256-307X/36/10/107402](#) (2019).
 - [41] T. Shang, C. Baines, L.-J. Chang, D. J. Gawryluk, E. Pomjakushina, M. Shi, M. Medarde, and T. Shiroka, Re₁ Mox as an ideal test case of time-reversal symmetry breaking in unconventional superconductors, *npj Quantum Materials* **5**, [10.1038/s41535-020-00279-1](#) (2020).
 - [42] P. K. Biswas, A. D. Hillier, M. R. Lees, and D. McK Paul, Comparative study of the centrosymmetric and noncentrosymmetric superconducting phases of Re₃ W using muon spin spectroscopy and heat capacity measurements, *Physical Review B* **85**, 134505 (2012).
 - [43] G. Aeppli, R. J. Cava Atd', E. J. Ansaldo, J. H. Brewer, S. R. Kreitzman, G. M. Luke, D. R. Noakes, and R. F. Kiefl, *Physical Review B*, Tech. Rep. (1987).
 - [44] E. Brandt, Properties of the ideal Ginzburg-Landau vortex lattice, *Physical Review B* **68**, 19 (2003).